Application of Color Mixing for Safety and Quality Inspection of Agricultural Products

Fujian Ding, Yud-Ren Chen, Kuanglin Chao

Instrumentation and Sensing Laboratory, ARS, USDA, Beltsville, MD, USA 20705-2350

ABSTRACT

In this paper, color-mixing applications for food safety and quality was studied, including two-color mixing and three-color mixing. It was shown that the chromaticness of the visual signal resulting from two- or three-color mixing is directly related to the band ratio of light intensity at the two or three selected wavebands. An optical visual device using color mixing to implement the band ratio criterion was presented. Inspection through human vision assisted by an optical device that implements the band ratio criterion would offer flexibility and significant cost savings as compared to inspection with a multispectral machine vision system that implements the same criterion. Example applications of this optical color mixing technique were given for the inspection of chicken carcasses with various diseases and for the detection of chilling injury in cucumbers. Simulation results showed that discrimination by chromaticness that has a direct relation with band ratio can work very well with proper selection of the two or three narrow wavebands. This novel color mixing technique for visual inspection can be implemented on visual devices for a variety of applications, ranging from target detection to food safety inspection.

Keywords. Band Ratio Criterion, Color Vision, Detection, Food Safety Inspection, Optical Instrument

Mention of trade names or commercial products is solely for the purpose of providing specific information and does not imply endorsement or recommendation by the USDA.

1. INTRODUCTION

Spectroscopy and multispectral imaging techniques have been applied for military target detection, natural resources assessment, and detection of diseases, defects, and contamination for food safety and quality. At the Instrumentation and Sensing Lab (ISL), we have applied these technologies to safety inspection of agricultural products[1-4]. The band ratio of reflectance intensity at two or three different wavelengths is invariant to geometric and illumination changes in the environment. Thus, the two-band ratio and three-band ratio criteria have been used effectively in a variety of target discrimination applications [5-8].

Band ratio criteria are used in digital image processing to enhance the contrast between selected features and superfluous features. These criteria are most often implemented in multispectral imaging systems, which generally use a beam splitter to create separate channels of light directed to separate CCD sensors, with the channels passing through band pass filters of different wavelengths. Ratio images are obtained by software algorithms. However, multispectral imaging systems are complicated and expensive. For application in processing plants, a low-cost visual device that can be used in existing environmental conditions would be preferred. At ISL, we are developing low-cost, optically enhanced devices that assist inspectors or plant processors in small meat and poultry plants to visually conduct inspection in-situ[9-10]. A visual inspection assistance device based on the two- or three-band ratio criterion can be implemented in a pair of binoculars equipped with a special two- or three-narrow-band interference optical filter. This device satisfies several requirements of in-situ inspection. First, the color extraction can be easily obtained. Second, by using the binoculars, there is enough angular resolution and brightness for inspection of objects from a distance. Third, the interference filter can be implemented in the optical binocular system easily due to the small field of view (FOV) of the binocular. Fourth, it is a portable personal device offering greater flexibility of use with a lower overall cost, compared to a multispectral imaging system. The schematic diagram of an optical device using the three-band ratio is shown in Figure 1.

Optical Sensors and Sensing Systems for Natural Resources and Food Safety and Quality, edited by Yud-Ren Chen, George E. Meyer, Shu-I Tu, Proc. of SPIE Vol. 5996, 59960R, (2005) · 0277-786X/05/$15 · doi: 10.1117/12.638037

By viewing through the optical assistance device, small plant operators can detect defective, diseased, and contaminated agricultural products, by identifying different colors resulting from the two or three-band ratio criterion. The special binocular can also enable an operator to inspect objects at a distance with enough resolution and sufficient brightness, for easier detection of some small targets, compared to the use of illuminating source optimization.

In this paper, a visual device to assist inspectors in identifying target conditions by utilizing two- or three-band ratio criterion is presented. The primary purpose of this paper is to present procedure and device needed to effectively implement the two- or three-band ratio criterion using an optical inspection method to aid human vision. We will establish the relationship between color attributes of the colors perceived through our special binocular and the two- or three-band ratio at two or three wavebands used in food safety inspection. The results can be used to train inspectors to identify the color associated with each target condition by simulating the colors of objects with known two- or three-band ratio values. This technique for visually reading the two- or three-band ratio is useful not only for food safety inspection, but also for target detection and for quality inspection in other fields. Seeing that the two-band application is a specific application of three-waveband application, here the theoretical analysis of the three-band application is given.

2. THEORY AND RELATION BETWEEN COLOR MIXING AND BAND RATIOS

2.1. Color Mixing

When an optical system is used in color perception, the tristimulus values *X, Y, Z* of an object color are given by[11]:

$$\begin{aligned} X &= k\sum_{\lambda} \tau_\lambda \rho_\lambda H_\lambda \bar{x}_\lambda \Delta\lambda \\ Y &= k\sum_{\lambda} \tau_\lambda \rho_\lambda H_\lambda \bar{y}_\lambda \Delta\lambda \\ Z &= k\sum_{\lambda} \tau_\lambda \rho_\lambda H_\lambda \bar{z}_\lambda \Delta\lambda \end{aligned} \tag{1}$$

Where $\bar{x}_\lambda$, $\bar{y}_\lambda$, $\bar{z}_\lambda$ are 1931 CIE color-matching functions, k is a normalizing factor, $H_\lambda \Delta\lambda$ is the spectral distribution of the flux irradiating the object, ρ_λ is the spectral reflectance of the object, and τ_λ is the transmittance of the optical system.

If three colors with tristimulus values (X_i, Y_i, Z_i) (i=1, 2, 3) and chromaticity coordinates (x_i, y_i, z_i) (i=1, 2, 3) are mixed together, a new color is produced which has chromaticity coordinates x_m, y_m, z_m that can be expressed as follows:

$$\begin{aligned} x_m &= \left(k_{12}x_1 + x_2 + k_{32}x_3\right)/\left(k_{12} + k_{32} + 1\right) \\ y_m &= \left(k_{12}y_1 + y_2 + k_{32}y_3\right)/\left(k_{12} + k_{32} + 1\right) \\ z_m &= \left(k_{12}z_1 + z_2 + k_{32}z_3\right)/\left(k_{12} + k_{32} + 1\right) \end{aligned} \tag{2}$$

where

$$k_{i2} = \left(X_i + Y_i + Z_i\right)/\left(X_2 + Y_2 + Z_2\right) \quad \left(i = 1, 3\right) \tag{3}$$

Equation 2 shows that the chromaticness (x_m, y_m, z_m) of the mixed colors will depend only on the chromaticity coordinates (x_i, y_i, z_i) (i=1, 2, 3) of the three colors, if the quantities, k_{12} and k_{32}, remain constant. The luminance after mixing, Y_m, is equal to the sum of Y_1, Y_2, and Y_3.

2.2. Band Ratios Criteria

The three-band ratio, C_{3br}, can be expressed with the indices as follows:

$$C_{3br} = E_{\lambda_1} : E_{\lambda_2} : E_{\lambda_3} \tag{4}$$

$$E_{\lambda_i} = \int_{\lambda_i-\Delta\lambda_i/2}^{\lambda_i+\Delta\lambda_i/2} F'(x_s, y_s, z_s)\tau'_\lambda \rho_\lambda H'_\lambda S_\lambda d\lambda \quad (i = 1, 2, 3) \tag{5}$$

where E_{λ_i} $(i = 1,2,3)$ are the energy in the unit time received by optical sensor at λ_i (i=1, 2, 3) respectively. F' is the geometrical function for a given optical system, τ'_λ is the spectral transmission of the optical system, H'_λ is the spectral radiant flux distribution of the lighting source, S_λ is the spectral responsivity of the optical sensor, and λ_1, λ_2 and λ_3 are the central wavelengths of the three bands. Since F' is the geometrical function, which remains constant for the three different wavelength bands of the same point on the object, so C_{3br} can be expressed as:

$$C_{3br} = \int_{\lambda_1-\Delta\lambda_1/2}^{\lambda_1+\Delta\lambda_1/2} \tau'_\lambda \rho_\lambda H'_\lambda S_\lambda d\lambda : \int_{\lambda_2-\Delta\lambda_2/2}^{\lambda_2+\Delta\lambda_2/2} \tau' \rho_\lambda H'_\lambda S_\lambda d\lambda : \int_{\lambda_3-\Delta\lambda_3/2}^{\lambda_3+\Delta\lambda_3/2} \tau'_\lambda \rho_\lambda H'_\lambda S_\lambda d\lambda \tag{6a}$$

Also, since in most applications the $\Delta\lambda_1$, $\Delta\lambda_2$, and $\Delta\lambda_3$ are small, the band ratio can be expressed by:

$$C_{3br} = \tau'_{\lambda_1} \rho_{\lambda_1} H'_{\lambda_1} S_{\lambda_1} \Delta\lambda_1 : \tau'_{\lambda_2} \rho_{\lambda_2} H'_{\lambda_2} S_{\lambda_2} \Delta\lambda_2 : \tau'_{\lambda_3} \rho_{\lambda_3} H'_{\lambda_3} S_{\lambda_3} \Delta\lambda_3 \tag{6b}$$

$$C_{3br} = C_{12} : 1 : C_{32} \tag{6c}$$

where $C_{12} = \dfrac{\tau'_{\lambda_1} \rho_{\lambda_1} H'_{\lambda_1} S_{\lambda_1} \Delta\lambda_1}{\tau'_{\lambda_2} \rho_{\lambda_2} H'_{\lambda_2} S_{\lambda_2} \Delta\lambda_2}$, $C_{32} = \dfrac{\tau'_{\lambda_3} \rho_{\lambda_3} H'_{\lambda_3} S_{\lambda_3} \Delta\lambda_3}{\tau'_{\lambda_2} \rho_{\lambda_2} H'_{\lambda_2} S_{\lambda_2} \Delta\lambda_2}$

Based on symmetric second difference (SSD) (Chen et al, 1998), where $\lambda_3 - \lambda_2 = \lambda_2 - \lambda_1$, the normalized symmetric second difference (NSSD), can be expressed by $\Delta_2 R(C_{12}, C_{32}) = C_{12} + C_{32} - 2$. Based on asymmetric second difference (ASD) (Mehl et al, 2004), we defined the normalized asymmetric second difference (NASD) by $\Delta_2 R(C_{12}, C_{32}) = k_1 C_{12} + k_2 C_{32} - 2$, where: $k_1 = 2\dfrac{\lambda_2 - \lambda_1}{\lambda_3 - \lambda_1}$, $k_2 = 2\dfrac{\lambda_3 - \lambda_2}{\lambda_3 - \lambda_1}$. For the normalized symmetric second difference (NSSD), k_1 and k_2 are equal to 1.0.

Equation 6 shows that the three-band ratio is independent of the geometrical functions, and, for a given system, it is only the function of the relative reflectance of the object, if the illuminating condition remains constant. This is also true for the normalized symmetric second difference and asymmetrical second difference. It can be concluded that the three-band ratio, C_{3br}, and the normalized second difference are not sensitive to the intensity variation in the illuminating lighting or background lighting, not sensitive to the objective distance between the optical system and the objects, and not sensitive to the angle between the optical axis and the normal line of the object surface. Hence, our goal was to develop the relationship between the three-band ratio and color attributes.

2.3. Relation between Band Ratio Criterion and Color Attributes

In this section, we will give the exact relation between the three-band ratio criterion and the chromaticness of the object color perceived through an optical device. As known, there are a number of color spaces including device dependent color spaces and device independent color spaces. There are two CIE based color spaces, CIELUV and CIELab. Both of these are device independent color spaces. In our application, the CIELUV was adapted in the theoretical analysis on the relation between the band ratio and color attributes.

When mixing three colors of small and equal bandwidths, $\Delta\lambda_1$, $\Delta\lambda_2$ and $\Delta\lambda_3$, Equations 3 and 6b can be used to give k_{i2} as follows:

$$k_{i2} = \frac{\tau_{\lambda_i} \tau'_{\lambda_2} H_{\lambda_i} H'_{\lambda_2} S_{\lambda_2} (\bar{x}_{\lambda_i} + \bar{y}_{\lambda_i} + \bar{z}_{\lambda_i})}{\tau_{\lambda_2} \tau'_{\lambda_i} H_{\lambda_2} H'_{\lambda_i} S_{\lambda_i} (\bar{x}_{\lambda_2} + \bar{y}_{\lambda_2} + \bar{z}_{\lambda_2})} C_{i2} \qquad (i = 1,\ 3) \tag{7a}$$

$$k_{i2} = c_i C_{i2} \quad (i = 1,\ 3) \tag{7b}$$

Where parameters c_1, c_3 remain constant.

In the CIELUV color space[11], the saturation, s^*_{uv}, and hue, h_{uv} , of a single target can be computed from its color coordinates (L^*, u^*, v^*), which, in turn, are computed from its tristimulus values (X, Y, Z) and normal reference white values (X_n, Y_n, Z_n) . The saturation and hue as are given as below:

$$s^*_{uv} = 13\left[(u' - u'_n)^2 + (v' - v'_n)^2\right]^{1/2} \tag{8}$$

$$h_{uv} = \arctan\left(v^* / u^*\right) \tag{9}$$

where u', v', u'_n, and v'_n are function of (X, Y, Z) and (X_n, Y_n, Z_n).[9]

In our application, s^*_{uv} and h_{uv} can be obtained as follows:

$$s^*_{uv} = \left[\left(\frac{a_1 + a_2 C_{12} + a_3 C_{32}}{a_4 + a_5 C_{12} + a_6 C_{32}}\right)^2 + \left(\frac{a_7 + a_8 C_{12} + a_9 C_{32}}{a_4 + a_5 C_{12} + a_6 C_{32}}\right)^2\right]^{1/2} \tag{10}$$

$$h_{uv} = \arctan\left(\left(a_1 + a_2 C_{12} + a_3 C_{32}\right) / \left(a_7 + a_8 C_{12} + a_9 C_{32}\right)\right) \tag{11}$$

or

$$C_{32} = \frac{d_1 + d_2 \cos(h_{uv}) s^*_{uv} + d_3 \sin(h_{uv}) s^*_{uv}}{d_4 + d_5 \cos(h_{uv}) s^*_{uv} + d_6 \sin(h_{uv}) s^*_{uv}} \tag{12}$$

$$C_{12} = \frac{d_7 \cos(h_{uv}) + d_8 \sin(h_{uv}) + s^*_{uv}\left[d_9 \cos(2h_{uv}) + d_{10} \sin(2h_{uv}) + d_{11}\right]}{d_{12} \cos(h_{uv}) + d_{13} \sin(h_{uv}) + s^*_{uv}\left[d_{14} \cos(2h_{uv}) + d_{15} \sin(2h_{uv}) + d_{16}\right]} \tag{13}$$

where a_1, a_2,…, a_9, d_1, d_2,…, d_{16} all are parameters, which are functions of the chromaticity (x_i, y_i, z_i) (i=1, 2, 3), (x_n, y_n, z_n), c_1 and c_3. The three-band ratio indices, C_{12} and C_{32}, are then only functions of the color attributes s^*_{uv} and h_{uv}. So the three-band ratio and the normalized second difference are the function of s^*_{uv} and h_{uv}. With the formulations of Equations 10 and 11, the saturation and the hue of a perceived object color can be calculated in terms of its three-band ratio indices. Equations 12 and 13 can be used to calculate the three-band ratio corresponding to specified color attributes of saturation and hue. Then the three-band ratio and the normalized second difference can be performed in term of the color attributes of the object colors.

All the above analysis is based on the three-band application. Being a specific case of the three-band application, the two-waveband application is the case when $C_{12} = 0$ or $C_{32} = 0$.

Seeing the fact that the two-waveband application is a subspace of the three-waveband application, generally speaking, a better solution can be found in the three-waveband space. But sometimes the two-waveband case is adequate for the application. When the color differences or chromaticness differences between targets and backgrounds are large enough to distinguish, the two-waveband is a choice due to its simplicity and low-cost. When the optimal solution is located in its a two-waveband subspace, then the two-waveband is the final choice.

2.4. Color and Chromaticness Differences Indices

Using the CIELUV color space[11], the color difference between two targets or between a target and its background is given as follows:

$$\Delta E\left(L^* u^* v^*\right) = \left[\left(\Delta L^*\right)^2 + \left(\Delta u^*\right)^2 + \left(\Delta v^*\right)^2\right]^{1/2} \tag{14}$$

The chromaticness difference index, $\Delta S'$, is defined as follows:

$$\Delta S' = 13\left[(\Delta u')^2 + (\Delta v')^2\right]^{0.5} \tag{15}$$

Both these indices take into account the difference in hue and saturation between two targets or a target and the background and can be also be used as a criterion for separating target and background.

3. COLOR SIMULATION ON THE COMPUTER

The color appearance model, the Revision of CIECAM97s for Practical Application proposed by Mark D. Fairchild[12], was applied to calculate the tristimulus values under the viewing condition in the simulation. This model can be used to convert from tristimulus values to perceptual attributes while the inverse model can be used to convert from perceptual attributes back to tristimulus values. The input and output viewing conditions are used during the forward and inverse calculations to account for differences in viewing condition. The procedure of the color simulation is shown in the flow chart in the Figure 2.

In the color simulation of the color chart on the computer, the device dependent color space RGB is applied. The color monitor (Sony Trinitron) was calibrated and profiled with GretagMacbeth Eye-One Display (GretagMacbeth, New Windsor, NY) before the simulation. The physical characteristics of this monitor are seen in the Tab.1. Color display monitors create different colors by additive mixtures of the three primaries R (red), G (green), and B (blue). The first step is to finish the transformation from (*X, Y, Z*) to (*R, G, B*). The transformation from (*X, Y, Z*) to (*R, G, B*) color space was performed by the following transformation matrix.

$$\begin{bmatrix} R \\ G \\ B \end{bmatrix} = M \begin{bmatrix} X \\ Y \\ Z \end{bmatrix} \tag{16}$$

Where $0 \le R \le 1$; $0 \le G \le 1$; $0 \le B \le 1$

The transformation matrix *M* for the monitor is:

$$M = \begin{bmatrix} 0.0485 & -0.0220 & -0.0072 \\ -0.0177 & 0.0323 & 0.0005 \\ 0.0009 & -0.0032 & 0.0169 \end{bmatrix}$$

The color on the monitor display produced by a particular RGB specification depends on the gamma characteristics of the display[13] and the input voltage for each R, G, or B channel. The simulation of using color-mixing binoculars to view chicken samples, taking into account monitor viewing conditions, was used to calculate the RGB specifications needed to display colors on the monitor as if viewed through binoculars. Given the gamma characteristics that were measured for the monitor (listed in Table 1), the input voltages could be calculated from the power function for display intensity,

$$V = \left(\frac{L}{L_{\max}}\right)^{(1/\gamma)} \tag{17}$$

where V is the normalized input voltage (0<V<1) for each R, G, or B channel, and L_{max} is the maximum achievable display intensity. The image function IMAGE from MATLAB was used for the color monitor display.

4. APPLICATION TO FOOD AND AGRICULTURE PRODUCT INSPECTION

4.1. Viewing Device and Active Lighting Used

A pair of low-cost 8×32 binoculars with a 7.5 FOV can be customized with an interference two- or three-band pass filter in front of the objective lens, as shown in Figure 1. The objects were illuminated with 5,000 lx using a D65, the adapting is 20% of the luminance of white in the adapting field, and only light passing through the binoculars'

special filters reached the viewer. Because "white" as seen through this device is different from "white" under the D65 standard, the color-simulation includes the condition that white is D65 with an adapting field luminance of 18 cd/m^2 with a Revision of the CIE color appearance model CIECAM97s proposed by Mark D. Fairchild.

All the computation results presented below are based on the conditions that (1) the optical transmissions of the visual device and the multispectral system are very similar in the visible range, and (2) the spectral energy distributions of the illuminating sources in the multispectral system application and the visual device application are CIE D65.

4.2. Application on Identification of Different Unwholesome Conditions of Chicken Carcasses

A total of 467 chicken carcasses (213 wholesome, 51 airsacculitis, 80 cadaver, 51 IP, 64 Septox, and 8 tumor) were obtained from the processing line at a poultry slaughter plant. The chicken spectra data used in this research is described in detail by Chao et al. (2004)[14].

The criterion for separating a single chicken condition, such as wholesome, from all other conditions is to maximize the chromaticness difference index $\Delta S'$ between the wholesome chickens and the unwholesome chickens. For differentiating between multiple chicken conditions, the objective of waveband optimization is to select the three-waveband set (λ_1, λ_2, λ_3) that maximizes the smallest chromaticness differences between all the multiple target conditions. A software for optimal waveband(s) selection is applied to one waveband, two waveband, or three waveband application. The flow chart of the waveband(s) optimal selection is shown in the Figure 3. With the respective initial parameter, waveband number *nw*, the software can give the optimal solution for one waveband, or two-waveband, or three-waveband application. When the function index number *nf* is set 0, then chromaticness difference index will be used as the function. If the function index number *nf* is set 1, then color difference will be used as the function.

Table 2 shows the optimal three-waveband sets for single condition detection and multiple condition detection. Table 3 shows the color differences for the multi-target detection using the three-wavelength set (447 nm, 522 nm, and 627 nm) and the two-wavelength set (454 nm, and 578 nm). Compared with using the two-color mixing application, the identification of the air-sac condition from the wholesome condition using the three-color mixing application becomes easier because the three-band color difference is as high as 5.05 while the two-band color difference is only 3.57. For the identification of the septox condition from the IP condition, the color difference greatly improves from 2.97 to 4.40 when using the three-band application instead of the two-band application, clearly making identification of septox from IP much easier. Clearly, the three-waveband application is the better choice for the multi-target inspection of chicken, since the two-waveband application does not identify septox from IP, or air-sac from wholesome, as well as the three-waveband application.

Table 4 shows the parameters that can be used in Equations 10, 11, 12, and 13 to obtain the values for saturation, hue and the band ratio indices. The related parameters k_1 and k_2, used in the normalized asymmetric second difference, are 0.833 and 1.167, respectively.

Table 5 shows, for each carcass condition, the band ratio indices and the saturation and hue values for the multi-target detection wavelength set (447 nm, 522 nm, and 627 nm), along with the normalized asymmetric second difference. The cadaver condition clearly shows the smallest hue value, differing very obviously from the hue values of the other conditions. The saturation of the tumor condition is greatest and obviously differs from all the other five conditions. These factors render the cadaver and the tumor colors the most distinct from the others. According to the value of the saturation and hue in CIELUV color space, the air-sac and wholesome conditions are the most similar conditions. In terms of the normalized asymmetric second differences, cadaver and tumor are each very distinct from all the other conditions. Air-sac and wholesome carcasses are close to each other in terms of the normalized asymmetric second difference. Comparing the normalized asymmetric second differences and the color attributes, we can come to the conclusion that there is a very good consistency between both of these criteria.

If the color difference between two different conditions is greater than 5.0,[15] it is considered to be easily differentiable by eye, while a color difference of 1.0 is considered to be only a noticeable color difference, under the CIE reference viewing condition[15]. Table 2 shows that all the six conditions can be easily identified with three-

waveband color mixing: the color difference between any two different conditions is always greater than 5.0, with only one exception that is still very close to being easily differentiable, the 4.40 color difference between IP and Septox. The color simulation for the two- and three-waveband multi-target applications for chicken carcasses are shown in the Figure 4. According to the color simulation, we can conclude that the different unwholesome and wholesome conditions of chicken carcasses are more easily identified using three-waveband color mixing. All six of the chicken carcass conditions can be distinguished from each other; in contrast, the IP and Septox conditions are not so easily separated using two-waveband color mixing as three-waveband color mixing.

4.3. Application for the Detection of Chilling Injury in Cucumbers

A group of cucumbers stored for 12 days at 0˚C was used for the wavelength pair selection process. Regions of Interest (ROI) were chosen from areas of (a) good-smooth skin of green color; (b) good-smooth skins of yellow color; (c) chilling injured skins of gray color; (d) chilling injured skins of black color; (e) chilling injured skins of white color; (f) chilling injured skins of black color; (g) chilling injured skins of gray color; (h) chilling injured skins of gray color. The relative reflectance of different conditions are shown in the Figure 5. Given the color variations evident for both good and injured skins, the selection of a waveband pair for detecting chilling injury was aimed to minimize the chromaticness difference between different good smooth skins while maximizing the chromaticness differences between chilling injury skins and good skins. The optimal wavelength pair based on the above procedure is 504 nm and 652 nm. The Training Color Chart of Chilling Injury and a simulated picture of the group chilling injury cucumbers are shown Figure 6 and Figure 7, respectively. According to the simulation of the group chilling injury cucumbers, the different chilling injury areas are easy to detect in term of the color differences at the wavelength pair 504 nm and 652 nm.

5. CONCLUSIONS

In food safety and quality inspection, it is important to have systems or devices that can help to effectively separate wholesome products from diseased or defective ones. The spectroscopic three-band ratio and its alternatives are powerful tools for discriminating among two or more classes. This paper presents a visual method of implementing the band ratio criterion. Using a two- or three-band-filter optical device, the extracted color is related to the two- or three-band ratio at the respective narrow wavebands. With this method, the inspector can identify the target in accordance to band ratio criterion.

The formulation between the saturation, hue, and band ratio is presented. The saturation and hue corresponding to different three-band ratio conditions of chicken carcasses are given. It was further demonstrated that the differences in the resultant mixed color among wholesome and diseased and defective chicken carcasses are large enough to be used for discrimination. This three-waveband application is more effective in the identification of the conditions of chicken carcasses than the two-waveband application. From the above examples, this kind of visual method can be used in classifying food and agricultural products for safety and quality. This research showed that it is feasible to develop a low-cost, binocular-based inspection device that will assist operators at processing plants to accurately detect defective, diseased and contaminated chicken carcasses at a distance with enough angular resolution. The three-color mixing technique can greatly improve the separation power of visual inspection. It also can be implemented in visual or binocular devices for detection of other types of target detection as long as the optimized three-band ratio criterion is one that works in the visible wavelength range.

REFERENCES

1. Chen, Y.R. and D.R. Massie. 1993. Visible/NIR reflectance and interactance spectroscopy for detection poultry carcasses. Transactions of the ASAE, 36(3):863-869.
2. Chen, Y.R. 1992. Classifying diseased poultry carcasses by visible and near-IR reflectance spectroscopy. Optics in Agriculture and Forestry, SPIE, 1836:44-55.
3. Chao, K., Y.R. Chen, W.R. Hruschka, and F.B. Gwozdz. 2002. On-line inspection of poultry carcasses by dual-camera system. Journal of Food Engineering. 51(3):185-192.
4. Kim, M.S., A.M. Lefcourt, and Y.R. Chen. 2003. Multispectral laser-induced fluorescence imaging system for large biological samples. Appl. Opt. 42(19):3927-3934.

5. Processing and Classification of Remotely Sensed Data; Pattern Recognition; Approaches to Data/Image Interpretation, http://rst.gsfc.nasa.gov/Front/tofc.html
6. Pu, R., S. Ge, N.M. Kelly and P. Gong. 2003. Spectral absorption features as indicators of water status in coast live oak (Quercus agrifolia) leaves. International Journal of Remote Sensing, 24(9):1799-1810
7. Gao, B.C. and A.F. Goetz. Extraction of Dry Leaf Spectral Features from Reflectance Spectra of Green Vegetation. Remote Sensing of Environment, 47, 369-274
8. Liew, S.C., A.S. Chia, L.K. Kwoh. 2001. Evaluating the validity of SeaWifs Chlorophyll algorithm for coastal waters. Proc. ACRS 2001 - 22nd Asian Conference on Remote Sensing, Singapore. 2:939-943.
9. Ding, F., Y. R. Chen, and K. Chao. 2005. Two-waveband color-mixing binoculars for the detection of wholesome and unwholesome chicken carcasses: a simulation. Appl. Opt. 44(26):5454-5462
10. Ding, F., Y. R. Chen, K. Chao, and D.E. Chan. 2005. Two-color mixing for classifying agricultural products for safety and quality" Appl. Opt. (in press).
11. Wyszecki, G. and W. S. Stiles, *Color Science: Concepts and Methods, Quantitative Data and Formulas.* Wiley, New York, 1982.
12. Fairchild, M.D. 2001. Revision of CIECAM97s for practical applications. Color Research and Application, 26:418-427.
13. Barco, L.J., J. A. Diaz, J. R. Jimenez, and M. Rubino. 1995. Considerations on the calibration of color displays assuming constant channel chromaticity. Color Res. Appl. 20:377-387.
14. Chao, K., Y.R. Chen, and D.E. Chan. 2004. A spectroscopic system for high-speed inspection of poultry carcasses. Applied Engineering in Agriculture. 20(5): 683-690.
15. International Commission on Illumination. Recommendation on Uniform Color Spaces, Color Difference Equations, Psychometric Color Terms. Supplement N0.2 to CIE publication N0.15 (E.-1.3.1), 1971/ (TC-1.3.), 1978

Table 1: Physical Characteristics of SONY Trinitron Color CRT Monitor

Max Luminance		62.28 cd/m^2
White Pixels RGB Values		255, 255, 255
CIE(x, y) Chromaticity Coordinates of White Pixels		0.3112, 0.3295
CIE(x, y) of the CRT's R Primaries		0.6261, 0.3426
CIE(x, y) of the CRT's G Primaries		0.2909, 0.6091
CIE(x, y) of the CRT's B Primaries		0.1479, 0.0698
gamma	R Primaries	2.133
	G Primaries	2.145
	B Primaries	2.117

Table 2: Visual Device Optimal Wavelength of Three Bands

Target Condition		Wavelengths (nm)		
		Band 1	Band 2	Band 3
Single-Target	Wholesome	417	462	594
	Air-sac	447	534	630
	Cadaver	414	531	648
	IP	456	588	645
	Septox	411	519	651
	Tumor	426	513	643
Multi-Target		447	522	627

Table 3: Multi-Target Color Differences Comparison

	Wholesome	Air-sac	Cadaver	IP	Septox	Tumor
Wholesome	0.0	5.05* 3.57**	27.4 26.5	10.2 10.7	9.39 11.0	20.2 11.9
Air-sac		0.0	29.5 25.9	12.6 10.4	9.91 9.66	15.2 8.36
Cadaver			0.0	17.2 15.8	19.7 16.4	41.1 24.6
IP				0.0	4.40 2.97	26.2 12.2
Septox					0.0	22.2 9.60
Tumor						0.0

*: Color difference at three waveband 447 nm, 522 nm, and 627 nm.
**: Color difference at two waveband 454 nm, and 578 nm.

Table 4: Parameters at the wavelength set: 447 nm, 522 nm, and 627 nm

parameters	values	Parameters	values	parameters	values
a_1	3.6108	c_1	16.4187	d_8	-1.4087
a_2	-0.73166	c_3	2.7148	d_9	-0.34209
a_3	1.1046	d_1	2.9637	d_{10}	-0.93523
a_4	-3.2352	d_2	1.5169	d_{11}	0.09302
a_5	-0.16523	d_3	0.54976	d_{12}	0.60063
a_6	1.3714	d_4	0.82092	d_{13}	-0.13564
a_7	12.82	d_5	-0.53302	d_{14}	-0.16463
a_8	2.8639	d_6	0.36754	d_{15}	0.1785
a_9	5.1472	d_7	6.2377	d_{16}	-0.22536

Table 5: Saturation, Hue and Band Ratio at the wavelength set: 447 nm, 522 nm, and 627 nm

Target Condition	parameters				
	C_{12}	C_{32}	S_{uv}^*	$H_{uv}(^\circ)$	$\Delta_2 R$
Air-sac	0.3810	1.911	1.256	59.14	0.548
Cadaver	0.4097	2.518	1.549	51.14	1.280
IP	0.4009	1.964	1.222	57.46	0.626
Wholesome	0.3871	1.929	1.246	58.60	0.574
Septox	0.3854	2.043	1.332	56.93	0.705
Tumor	0.2883	2.300	1.862	57.17	0.924

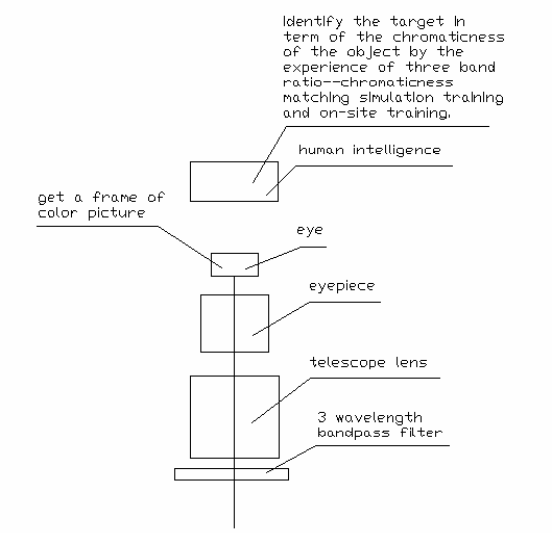

Figure 1: The schematic of implementation of the three-band ratio criterion with three-color mixing

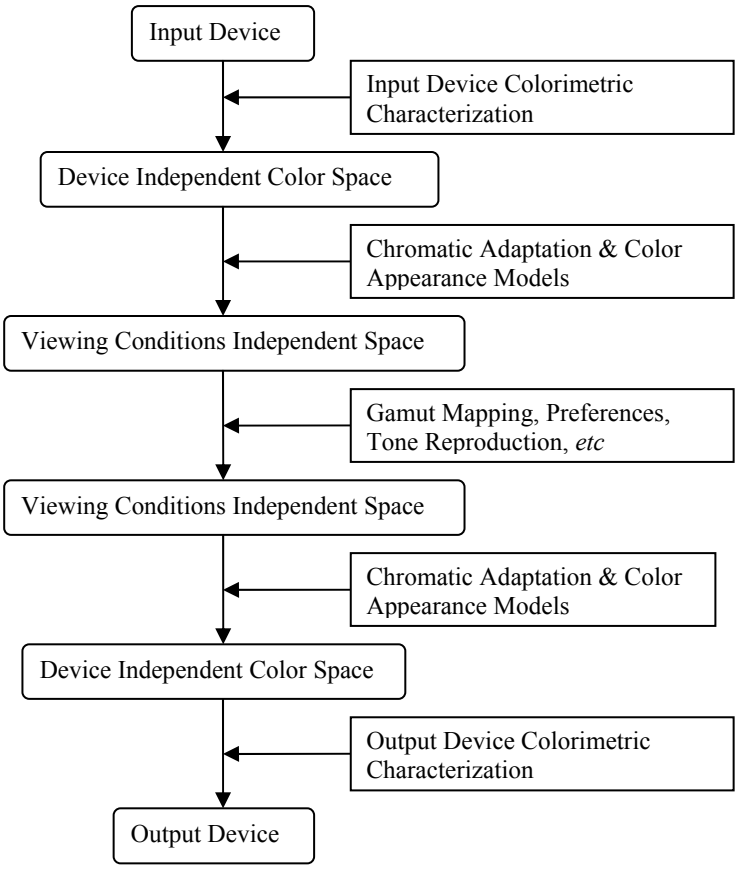

Figure 2: Flow chart of the process of device-independent color imaging

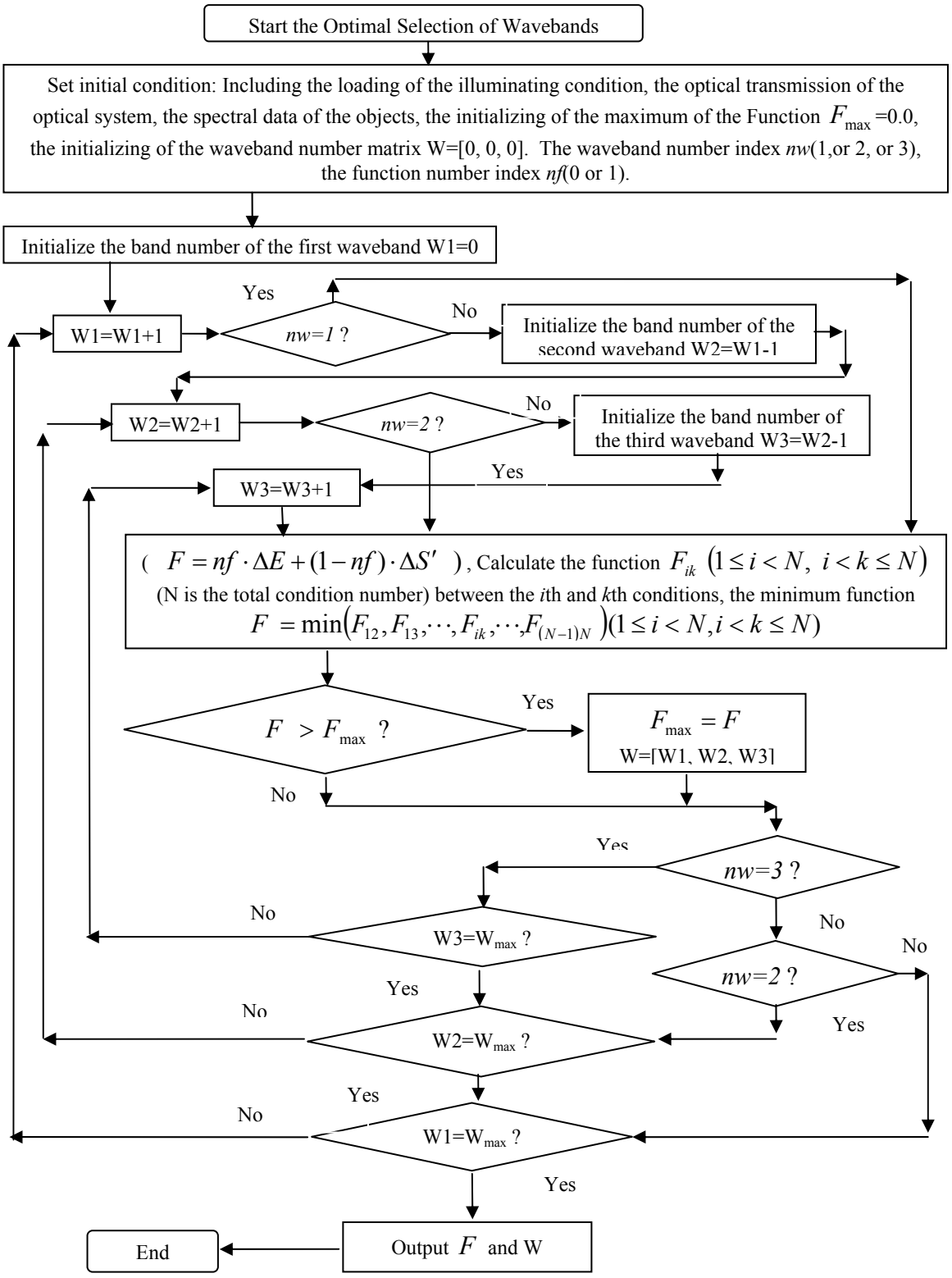

Figure 3: Flow Chart of the algorithm for the selection of the optimal waveband(s)

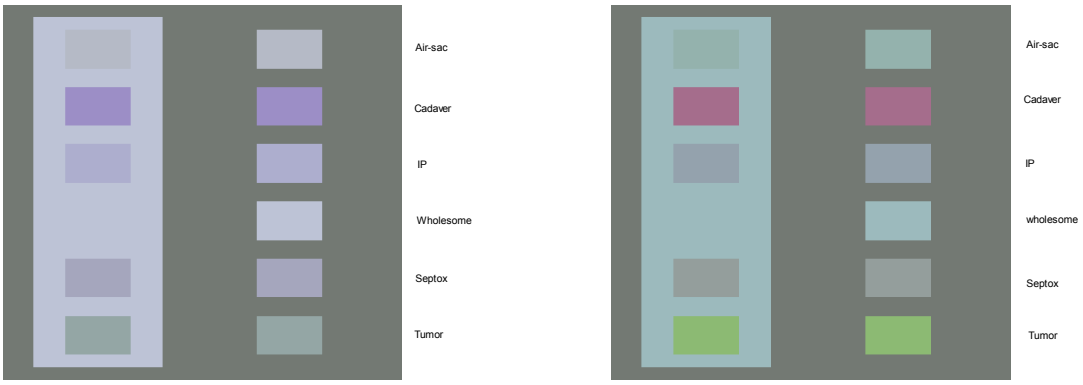

(a) (b)

Figure 4: Color Simulation of the Chicken Carcasses at: (a) two waveband; (b) three waveband

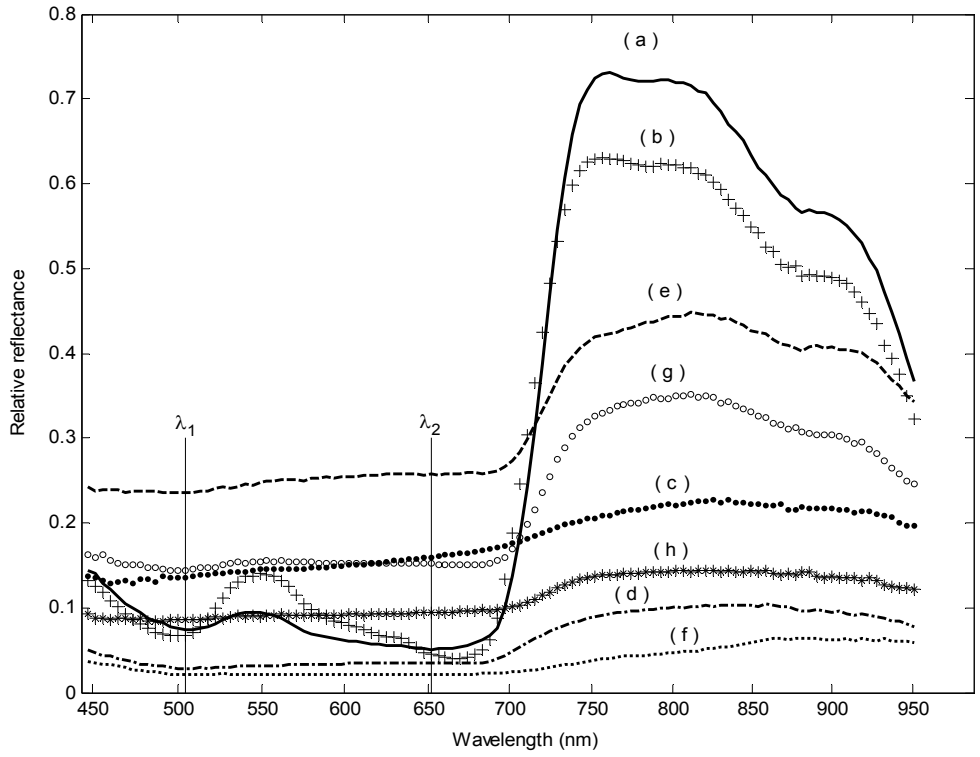

Figure 5: Relative Reflectance of Chilling Injury in Cucumbers: (a) Good-smooth skin of green color; (b) Good-smooth skins of yellow color; (c) Chilling injured skins of gray color; (d) Chilling injured skins of black color; (e) Chilling injured skins of white color; (f) Chilling injured skins of black color; (g) Chilling injured skins of gray color; (h) Chilling injured skins of gray color

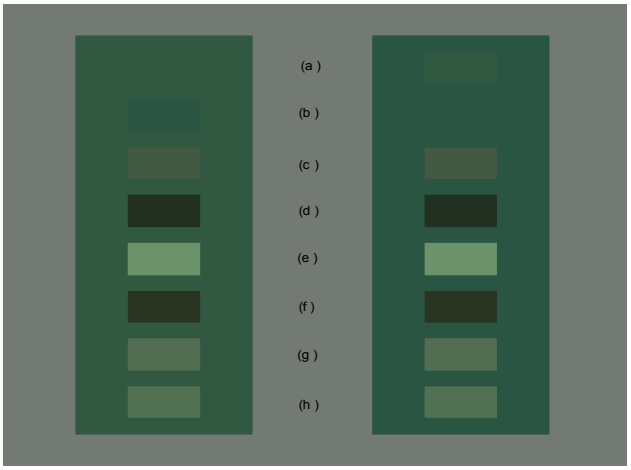

Figure 6: Training Color Chart of Chilling Injury: (a) Good-smooth skin of green color; (b) Good-smooth skins of yellow color; (c) Chilling injured skins of gray color; (d) Chilling injured skins of black color; (e) Chilling injured skins of white color; (f) Chilling injured skins of black color; (g) Chilling injured skins of gray color; (h) Chilling injured skins of gray color

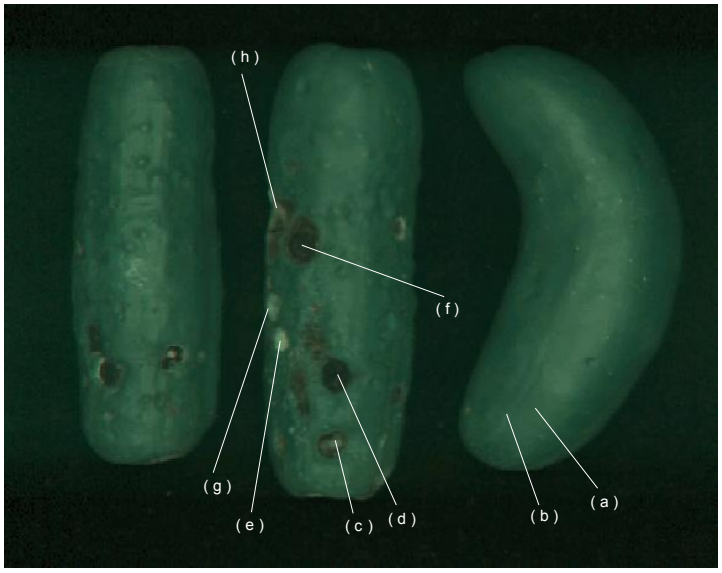

Figure 7: A Simulated Picture of one Group Chilling Injury Cucumbers: (a) Good-smooth skin of green color; (b) Good-smooth skins of yellow color; (c) Chilling injured skins of gray color; (d) Chilling injured skins of black color; (e) Chilling injured skins of white color; (f) Chilling injured skins of black color; (g) Chilling injured skins of gray color; (h) Chilling injured skins of gray color